cases have shown equal reactivity toward ethylene conversion, and therefore we would expect similar results from experiments such as those described here.

Conclusions

Thermal desorption of deuterated or partially deuterated chemisorbed ethylene on Pt(111), together with kinetic measurements using NEXAFS, have given us new insights on the mechanism of ethylidyne formation. The kinetic studies show that the limiting step of the reaction is unimolecular and that there is a normal isotope effect in the reaction rates between hydrogen and deuterium. It is also clear that if the process does not occur in one elementary step, the first is the rate limiting. TDS results using a C_2D_4:C_2H_4 mixture proved that the reaction is indeed intramolecular, as we would have expected from an unimolecular process. Finally, the experiments using $CHD{=}CD_2$ indicate that the hydrogen atom involved in the slow step is the same that desorbs first in the thermal desorption. This rules out ethylidene as an intermediate, and we propose the formation of vinyl as a transient moiety on the surface.

Acknowledgment. We want to thank Professor Thomas Morton for his assistance in the synthesis of trideuterioethylene. This work was supported in part by NSF Grant CHE 88-02086.

Registry No. C_2H_4, 74-85-1; C_2H_3, 67624-57-1; Pt, 7440-06-4.

(27) Windham, R. G.; Bartram, M. E.; Koel, B. E. 33rd National Symposium of the American Vacuum Society, Baltimore, 1986.

Calculation of Excited-State Geometries via the Time-Dependent Theory of Resonance Raman Spectroscopy: Application to Complexes of the Type $Rh_2(O_2CCH_3)_4(MPh_3)_2$, M = P, As, or Sb, at Resonance in Each Case with the Lowest $^1A_{2u}$ Excited State

Kyeong-Sook Shin,[1a] Robin J. H. Clark,*[1b] and Jeffrey I. Zink*[1a]

Contribution from the Department of Chemistry and Biochemistry, University of California, Los Angeles, Los Angeles, California 90024, and Christopher Ingold Laboratories, University College London, 20 Gordon Street, London WC1H 0AJ, England. *Received October 13, 1988*

Abstract: The calculation of both the excitation profiles of all the resonance-enhanced Raman bands and the intensities of all the observed overtone and combination bands of the rich resonance Raman spectra of the axially disubstituted dirhodium tetraacetate complexes $Rh_2(O_2CCH_3)_4(MPh_3)_2$, M = P, As, or Sb, is reported. The calculation uses the time-dependent theory of Lee and Heller. The geometric changes attendant upon excitation of each molecule from the ground to the first excited state, i.e. at resonance with the lowest $^1A_{2u} \leftarrow {}^1A_{1g}$ transition, are calculated. All the excitation profiles and the resonance Raman spectra are fitted by use of a single set of parameters, Δ (the displacement in dimensionless normal coordinates), E_{00} (the zero–zero electronic transition wavenumber), and Γ (the damping factor). The largest bond length changes in all of the molecules are in the Rh–Rh and Rh–O bonds.

The calculation of the geometries of molecules and ions in excited electronic states from resonance Raman spectra has traditionally been carried out via a Franck–Condon analysis of the intensities of Raman bands in spectra for which ω_I (the excitation line wavenumber) coincides with ω_0 (the wavenumber of the electronic transition in question).[2] Examples of such analyses include cases in which the resonant band is structured (e.g. MnO_4^-)[3] as well as unstructured (e.g. S_2^-).[4] An alternative treatment of resonance Raman data with certain advantages over the Franck–Condon treatment is that based on the transformation of the Kramers–Heisenberg–Dirac formula to the time domain, viz. the Lee–Heller treatment.[5] The distortions of a variety of metal-containing compounds have been calculated by use of preresonance Raman intensities and the applicable short-time approximation of the theory.[6-12]

The present paper is concerned with the results of the time-dependent analysis of excitation profiles and resonance Raman spectra applied to a set of complexes that are known to display particularly rich resonance Raman spectra. These are dirhodium tetraacetate complexes which are diaxially substituted with group V ligands, viz. $Rh_2(O_2CCH_3)_4(MPh_3)_2$, M = P, As, or Sb. Such complexes have the skeletal D_{4h} structure illustrated below (L = MPh_3, R = CH_3).

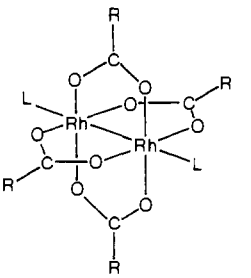

(1) (a) Department of Chemistry and Biochemistry, University of California, Los Angeles. (b) Christopher Ingold Laboratories, University College London.
(2) Clark, R. J. H.; Dines T. J. *Angew. Chem. Int. Ed. Engl.* **1986**, *25*, 131.
(3) Clark, R. J. H.; Stewart, B. *J. Am. Chem. Soc.* **1981**, *103*, 6593.
(4) Clark, R. J. H.; Dines, T. J.; Kurmoo, M. *Inorg. Chem.* **1983**, *22*, 2766.
(5) Tannor, D.; Heller, E. *J. Phys. Chem.* **1982**, *77*, 202.
(6) Tutt, L.; Zink, J. I. *J. Am. Chem. Soc.* **1986**, *108*, 5830.
(7) Yang, Y. Y.; Zink, J. I. *Inorg. Chem.* **1985**, *24*, 4012.
(8) Zink, J. I. *Coord. Chem. Rev.* **1985**, *64*, 93.
(9) Tutt, L.; Tannor, D.; Schindler, J.; Heller, E. J.; Zink, J. I. *J. Phys. Chem.* **1983**, *87*, 3017.
(10) Yoo, C. S.; Zink, J. I. *Inorg. Chem.* **1983**, *22*, 2474.
(11) Yang, Y. Y.; Zink, J. I. *J. Am. Chem. Soc.* **1984**, *106*, 1501.
(12) Zink, J. I.; Tutt, L.; Yang, Y. Y. *Adv. Chem. Ser.* **1986**, *307*, 39.

0002-7863/89/1511-4244$01.50/0

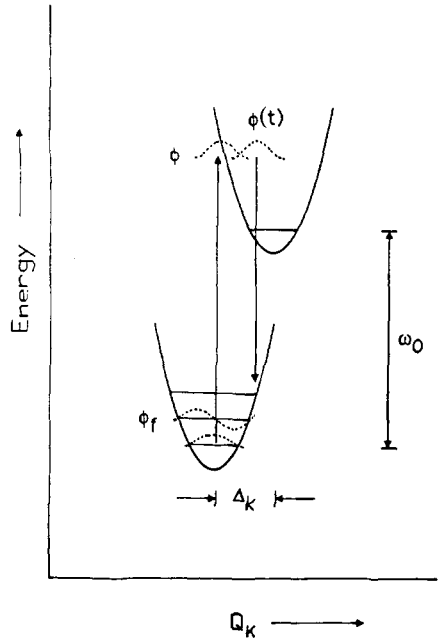

Figure 1. Illustration of time-dependent theory of resonance Raman scattering. ϕ is the initial wave packet, $\phi(t)$ is the moving wave packet, and ϕ_f is the final state of interest.

Detailed resonance Raman spectra of these complexes, including those of the ^{18}O and CD_3 isotopomers of the triphenylphosphine complex, have been recorded, and assignments for the key skeletal modes have been made.[13-15] The present paper is the first quantitative analysis of the geometric changes attendant upon excitation into the lowest allowed electronic state (ca. 370 nm), the transition being known to be axially polarized[13,14] and thus considered to be the lowest $^1A_{2u} \leftarrow {}^1A_{1g}$ transition with largely $d_{z^2} \leftarrow d_{z^2}$ ($\sigma^*(Rh_2) \leftarrow \sigma(Rh_2)$) parentage.[16,17] The present results, however, demonstrate that there is also significant $d_{x^2-y^2} \leftarrow d_{x^2-y^2}$ and possibly other parentage to this transition.

Experimental Section

The details on the Raman spectra of the complexes have been reported elsewhere.[13-15] The intensities of each resonance-enhanced band at each available excitation wavelength have been estimated from the products of the peak heights and full-widths at half-height (triangular approximation). The relative intensities of all the peaks in a resonance Raman spectrum were estimated from the peak height. All intensity data were corrected for frequency factors and also for the spectral response of the instrument (gratings, photomultiplier, etc.) by use of a tungsten strip lamp standardized at the National Physical Laboratory. The internal intensity standard in each case was the $\nu_1(a_1')$ band of KNO_3 at 1049 cm^{-1}.

Theory

The theoretical treatment of the resonance Raman data is based on the time-dependent theory of Lee and Heller. The calculation in the time domain is very efficient because the evaluation of Franck–Condon (F–C) factors and the sum over states can be avoided. The intensities of a large number of vibrational bands including overtone and combination bands can readily be calculated.

The Raman scattering amplitude (polarizability) is given by[18]

$$[\alpha_{fi}] = \frac{i}{\hbar}\int_0^\infty \langle\phi_f|\phi(t)\rangle \exp\{(i\omega' - \Gamma)t\}\, dt \qquad (1)$$

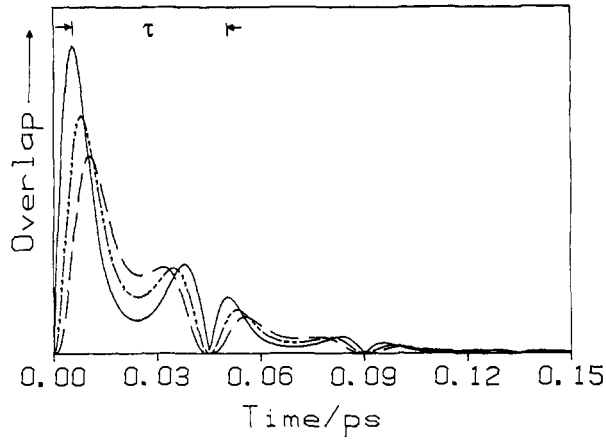

Figure 2. Magnitude of damped overlaps for f = 1–3, $|\langle\phi_f|\phi(t)\rangle \exp(-\Gamma t)|$, versus time: ν_1 (—), $2\nu_1$ (–··–), and $3\nu_1$ (––).

where $|\phi_f\rangle = \mu|\chi_f\rangle$ is the final vibrational state of the ground electronic surface multiplied by the transition electric dipole moment, $|\phi(t)\rangle = \exp(-iH_{ex}t/\hbar)|\phi\rangle$ is a moving wave packet propagated by the excited-state Hamiltonian, $|\phi\rangle = \mu|\chi\rangle$ is the initial vibrational state of the ground electronic surface multiplied by the electronic transition moment, Γ is the damping factor, $\omega' = \omega_i + \omega_l$, $\hbar\omega_i$ is the zero-point energy of the ground electronic surface, and $\hbar\omega_l$ is the energy of the incident radiation.

The resonance Raman scattering amplitude is governed by the motion of a wave packet on a multidimensional hypersurface representing the electronic state potential. A cross section of a multidimensional surface along one normal mode, which will be used to discuss the theory, is shown in Figure 1.

The initial wave packet, ϕ, makes a vertical transition onto the potential surface of the excited state, which, in general, is displaced relative to that of the ground state. The displaced wave packet is not a stationary state and evolves according to the time-dependent Schrödinger equation. The quantity of interest is the overlap of the moving wave packet $\phi(t)$ with the final state of interest ϕ_f. ϕ_f is the wave function of the normal mode k with vibrational quantum number n_k. If it is assumed that (a) only one electronic excited state is involved, (b) the potential surfaces are harmonic, (c) the normal coordinates are not mixed in the excited state, (d) the transition dipole moment, μ, is constant, and (e) the force constants do not change in the excited state, then the overlap has the simple form

$$\langle\phi_f|\phi(t)\rangle = \prod_k \left\{ \exp\left[-\frac{\Delta_k^2}{2}(1 - \exp(-i\omega_k t)) - \frac{i\omega_k t}{2} \right] (1 - \exp(-i\omega_k t))^{n_k} \frac{(-1)^{n_k}\Delta_k^{n_k}}{(2^{n_k} n_k!)^{1/2}} \right\} \exp(-i\omega_0 t) \qquad (2)$$

In eq 2, ω_0 is the wavenumber of the zero–zero electronic transition (E_{00}) in reciprocal centimeters, ω_k and Δ_k are, respectively, the wavenumber in reciprocal centimeters and the displacement of the kth normal mode, and n_k is the vibrational quantum number of the kth normal mode in the ground electronic state (n_k = 0, 1, etc.). Equation 2 is used to calculate the cross sections for the fundamentals and all the various overtone and combination bands. For example, in order to calculate the cross section of the combination band ($\nu_1 + \nu_2$) in a three-mode case, $n_1 = 1$, $n_2 = 1$, and $n_3 = 0$.

The Raman scattering amplitude in the frequency domain is the half Fourier transform of the overlap in the time domain as shown in eq 1. The Raman intensity $I_{i\to f}$ into a particular mode f is

$$I_{i\to f} \propto \omega_l\omega_s^3[\alpha_{fi}][\alpha_{fi}]^* \qquad (3)$$

(13) Clark, R. J. H.; Hempleman, A. J.; Flint, C. D. *J. Am. Chem. Soc.* **1986**, *108*, 518.
(14) Clark, R. J. H.; Hempleman, A. J. *Inorg. Chem.* **1988**, *27*, 2225.
(15) Clark, R. J. H.; Hempleman, A. J. *Inorg. Chem.* **1989**, *28*, 92; **1989**, *28*, 746. *Croat. Chem. Acta* **1988**, *61*, 313.
(16) Bursten, B. E.; Cotton, F. A. *Inorg. Chem.* **1981**, *20*, 3042.
(17) Sowa, T.; Kawamura, T.; Shida, T.; Yonezawa, T. *Inorg. Chem.* **1983**, *22*, 56.

(18) This equation comes from the transformation of the Kramers–Heisenberg–Dirac (KHD) formula to the time domain (see ref 5).

where ω_s is the frequency of scattered radiation.

The example of a one normal-mode problem illustrates many of the important features of the calculation. The magnitudes of damped overlaps for $f = 1-3$, $|\langle\phi_f|\phi(t)\rangle \exp(-\Gamma t)|$, are plotted versus time in Figure 2. Since there is only one mode in this example, f is characterized by vibrational quantum number n_k only. At time zero, ϕ makes a vertical transition to the upper surface. The overlaps $\langle\phi_f|\phi(t)\rangle$ at $t = 0$ are identically zero because ϕ and ϕ_f are orthogonal eigenfunctions. However, ϕ is not an eigenfunction of the upper surface and begins to evolve on the upper surface according to the time-dependent Schrödinger equation. There is a peak in $|\langle\phi_f|\phi(t)\rangle|$ after $\phi(t)$ has moved away from the F–C region. The maximum overlap occurs after a longer time for overtones than for fundamentals as shown in Figure 2. The larger the value of n_k, the later the time at which the first maximum of the overlap occurs. The maximum is followed by a decrease as $\phi(t)$ moves further away. On the other hand, $\phi(t)$ will return to its initial position at time τ after one vibrational period. Each return is responsible for an additional peak. There are two maxima in $|\langle\phi_f|\phi(t)\rangle|$ as the wave packet both goes from and comes back to its initial position. The classical turning point falls between these maxima. At the end of each vibrational period, $\phi(t)$ and ϕ_f are once again orthogonal and $|\langle\phi_f|\phi(t)\rangle|$ drops to zero. In the frequency domain (the excitation profile), the vibronic spacing ω is equal to $2\pi/\tau$.

Critical Features in the Calculation

The calculated resonance Raman spectra and the excitation profiles are very sensitive to two important factors, the displacement Δ_k and the damping factor Γ. The physical meaning of these factors and the reasons for their effect on the calculated intensities are discussed in this section.

Effect of Δ_k. The first factor to be considered is the displacements (Δ_k) of the minima of the potential surfaces in the excited state relative to those in ground state. The bandwidth of the excitation profile for the kth mode increases with increasing displacement Δ_k. When the excitation profiles are smooth, the Raman intensities of fundamental and overtone bands measured at any given excitation wavelength increase with increasing displacements. The relative intensities of overtone bands to fundamentals also increase as displacements increase. When the excitation profiles are highly structured, there is no simple relationship between displacements and Raman intensities at any given excitation wavenumber. In that case, the complete excitation profiles have to be calculated to obtain accurate information about the displacements.

When there is more than one mode involved, those that have the largest displacements are the most likely to give rise to combination bands. The overlap in the time domain of a combination band is given by the product of the overlap of each mode involved in the combination band (when there is no coupling between the vibrational coordinates, which form the combination band). For example, the overlap of the combination band $\nu_1 + \nu_2$ is given by $\langle\phi_{11}|\phi_{10}\rangle\langle\phi_{21}|\phi_{20}\rangle$. Because of the appreciable magnitude of the overlap for the progression-forming mode, the overlap of the combination band can also have sufficient magnitude to give detectable Raman intensity. Thus, when there is a long progression of overtones of one mode ($n_1\nu_1$), it is also possible that the combination bands ($n_1\nu_1 + \nu_k$) will be found.

Effect of Γ. The second factor that critically affects the calculation of Raman intensities and excitation profiles, especially for overtone and combination bands, is the damping factor Γ. For a given displacement, the intensities of overtone and combination bands with respect to those of the fundamentals decrease when the damping factor increases. The reason for this decrease can be understood from the plot of the overlap in the time domain shown in Figure 2. The first recurrence of the overlap of an overtone occurs at a later time than that of the fundamental. The damping factor is an exponential decay function in the time domain. When the overlap is multiplied by the decay, the magnitude of the overlap at longer times is decreased more rapidly than that at shorter times. Therefore, the magnitude of the overlap of overtones suffers more reduction than that of fundamentals as the damping factor is increased. This reduction in the magnitude of overlap results in lower Raman intensity in the frequency domain when the time correlation function is half Fourier transformed. The same arguments also apply to combination bands. The effect of the damping factor on the Raman intensities of overtone and combination bands is quantitatively discussed below.

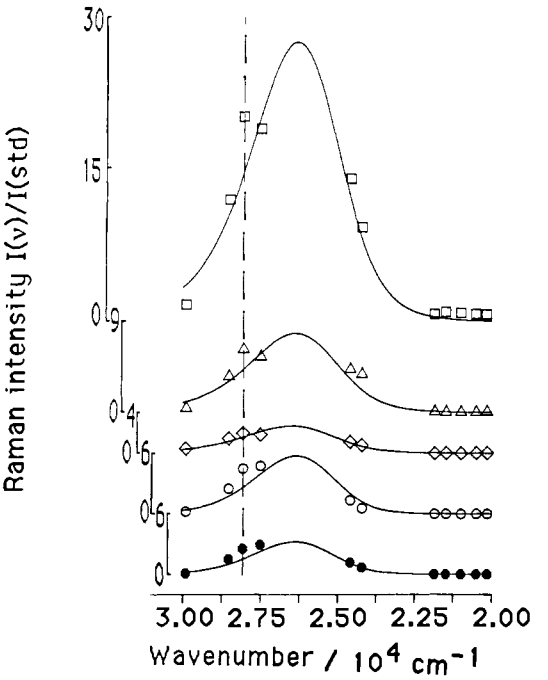

Figure 3. Calculated (—) and experimental resonance Raman excitation profiles of ν_1 (□), ν_2 (△), ν_3 (◇), $2\nu_1$ (○), and $\nu_1 + \nu_2$ (●) for $Rh_2O_2CCH_3(PPh_3)_2$.

Application of the Theory to $Rh_2(O_2CCH_3)_4L_2$, L = PPh_3, $AsPh_3$, $SbPh_3$

Calculation of the Excitation Profiles and Resonance Raman Spectra. The resonance Raman spectra and the excitation profiles of $Rh_2(O_2CCH_3)_4L_2$, L = PPh_3, $AsPh_3$, or $SbPh_3$, are calculated by using the time-dependent theory, which was described previously. The resonance Raman excitation profiles are calculated for a given set of values, Δ_k, ω_k, ω_I, Γ, and E_{00}, by use of eq 1 and 2. E_{00} is estimated from the electronic absorption spectrum, and the ω_k's are determined from the Raman spectrum. ω_I is the excitation wavenumber used to obtain the resonance Raman spectrum. The variable parameters are Δ_k and Γ.[19] Only one set of parameters is used for each complex to calculate all of the excitation profiles for the fundamental, overtone, and combination bands and to calculate the resonance Raman spectrum at a given excitation wavelength.

$Rh_2(O_2CCH_3)_4(PPh_3)_2$. The excitation profiles of best fit for the fundamentals ν_1, ν(Rh–Rh), ν_2, ν(Rh–O), and ν_3, y X-sens band, the overtone $2\nu_1$, and the combination band $\nu_1 + \nu_2$ for $Rh_2(O_2CCH_3)_4(PPh_3)_2$ are shown in Figure 3. They are calculated by using the parameters given in Table I. The calculated profiles are compared with the experimental values. This calculation involves nine vibrational modes. The calculated and experimental excitation profiles are in excellent agreement, not only with the bandwidth and shape of each excitation profile but also with the relative intensities obtained experimentally. All calculated excitation profiles are normalized to the maximum of

(19) When the resonance Raman excitation profiles are smooth and unstructured, the intensities from a given resonance Raman spectrum can be used to estimate the relative displacements. The initial estimates of the values of Δ to be used in the calculation of the Raman band excitation profiles are obtained from Savin's formula[20] by using the resonance Raman intensities.

(20) Heller, E. J.; Sundberg, R. L.; Tannor, D. *J. Phys. Chem.* **1982**, *86*, 1822.

Table I. Calculated Displacements Δ_k's for $Rh_2(O_2CCH_3)_4L_2$

	ω_k, cm^{-1}	assignt	Δ_k[a]
L = PPh_3[b]	289	ν_1(Rh–Rh)	3.73
	305	(Rh–O)	0.51
	320	(Rh–O)	0.48
	338	ν_2(Rh–O)	1.70
	521	y X-sens	0.65
	725	δ(OCO)	0.15
	1001	p-ring	0.14
	1099	q X-sens	0.17
	1588	k ν(C–C)	0.10
L = $AsPh_3$[c]	297	ν_1(Rh–Rh)	3.60
	321	(Rh–O)	0.66
	332	(Rh–O)	0.82
	342	ν_2(Rh–O)	2.03
	723	δ(OCO)	0.30
	1000	p-ring	0.16
L = $SbPh_3$[d]	277	ν_3(t X-sens)	2.61
	307	ν_1(Rh–Rh)	3.38
	339	ν_2(Rh–O)	3.14
	723	δ(OCO)	0.48
	998	p-ring	0.27
	1075	q X-sens	0.17
	1580	k ν(C–C)	0.11

[a] The Δ_k's are the displacements of the dimensionless normal coordinates. [b] E_{00} = 23 400 cm^{-1}[e] and Γ = 1350 cm^{-1}. [c] E_{00} = 25 000 cm^{-1}[e] and Γ = 897 cm^{-1}. [d] E_{00} = 22 050 cm^{-1}[e] and Γ = 800 cm^{-1}. [e] Estimated from the electronic absorption spectrum.

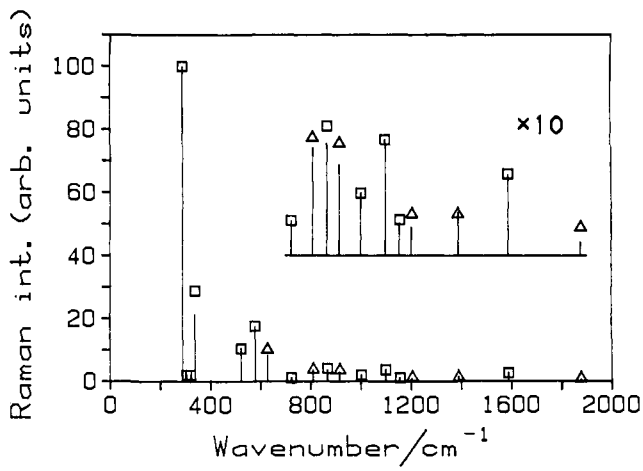

Figure 4. Calculated and experimental resonance Raman spectrum of $Rh_2O_2CCH_3(PH_3)_2$ at 356.4-nm excitation: (—) experimental intensities; (□, △) calculated intensities.

the ν_1 band. The maxima of all of the calculated excitation profiles are at 26 400 cm^{-1}, which corresponds to the maximum of the electronic absorption band with which the laser line is in resonance.

The calculated intensities for all of the observed fundamental, overtone, and combination bands at the excitation wavelength 356.4 nm (ω_l = 28 058 cm^{-1}) are compared to the experimental resonance Raman spectrum in Figure 4. The set of cross sections of excitation profiles for all modes at this laser wavelength forms the resonance Raman spectrum. The intensities at 356.4 nm excitation in the Raman excitation profiles are represented by a vertical broken line in Figure 3. The Raman intensities in the experimental spectrum are represented by vertical solid lines in Figure 4. The calculated intensities are represented by squares and triangles. The numerical values of calculated Raman band intensities are compared to the experimental values in Table II. The calculated resonance Raman intensities are in good agreement with those in the experimental spectrum.

The principal progression-forming mode, ν_1, is almost harmonic up to vibrational quantum number 6, with the anharmonicity constant $x_{11} \leq 0.2$ cm^{-1}. The overtone band wavenumbers derived from the calculation differ from the experimental values by a few wavenumbers as the vibrational quantum number increases. Other modes show only one or two harmonics. The assumption used in the calculation that the potential surfaces are harmonic is reasonable for this molecule.

Table II. Calculated and Observed Resonance Raman Intensities for $Rh_2(O_2CCH_3)_4(PPh_3)_2$

calcd intens[a]	obsd intens	ω_k, cm^{-1}	assignt
100.0	100.0	289	ν_1(Rh–Rh)
2.1	2.0	305	(Rh–O)
2.0	2.0	320	(Rh–O)
28.8	21.1	338	ν_2(Rh–O)
10.5	10.5	521	ν_3(y X-sens)
17.6	17.3	578	$2\nu_1$
10.2	8.2	627	$(\nu_1 + \nu_2)$
1.1	1.1	725	δ(OCO)
3.7	3.4	809	$(\nu_1 + \nu_3)$
4.1	3.5	866	$3\nu_1$
3.6	2.9	915	$(2\nu_1 + \nu_2)$
2.0	2.0	1001	p-ring
3.7	3.7	1099	q X-sens
1.1	1.0	1154	$4\nu_1$
1.3	0.9	1202	$(3\nu_1 + \nu_2)$
1.3	1.4	1389	ν_1 + q X-sens
2.6	2.6	1588	k ν(C–C)
0.9	0.4	1877	ν_1 + k ν(C–C)

[a] Calculated by using the parameters in Table I.

The damping factor used in the calculation is 1350 cm^{-1}. It is determined by the best fit of the resonance Raman intensities of the overtone and the combination bands. Changing the damping factor by 200 cm^{-1} significantly affects the fit to the intensities of the overtone and the combination bands. When the damping factor is increased to 1550 cm^{-1}, for example, the calculated intensities of the overtone and combination bands are decreased by more than 10%. This change becomes bigger as the vibrational quantum numbers of the overtone and combination bands increase. For example, the intensities of $2\nu_1$, $\nu_1 + \nu_2$, and $\nu_1 + \nu_3$ are decreased by about 11% compared to the intensities when the damping factor is 1350 cm^{-1}. The intensities of $3\nu_1$ and $2\nu_1 + \nu_2$ are decreased by about 19% and the intensities of $4\nu_1$ and $3\nu_1 + \nu_2$ are decreased by about 24%. However, the fit to the fundamentals is hardly affected.

The plots of the overlaps versus time in the time domain for any of the modes for $Rh_2(O_2CCH_3)_4(PPh_3)_2$ do not have significant recurrences. The damping factor is big enough to damp out all the recurrences, and the wave packet never returns to its original position after it moves away from the Franck–Condon region. The damping factors of the $Rh_2(O_2CCH_3)_4(AsPh_3)_2$ and $Rh_2(O_2CCH_3)_4(SbPh_3)_2$ complexes are also big enough to prevent significant recurrences.

$Rh_2(O_2CCH_3)_4(AsPh_3)_2$. The best fit excitation profiles of the fundamentals ν_1, ν_2, δ(OCO), the overtones $2\nu_1$, $2\nu_2$, and the combination tone $\nu_1 + \nu_2$ for $Rh_2(O_2CCH_3)_4(AsPh_3)_2$ are shown in Figure 5. They are calculated by using the parameters given in Table I. The calculated excitation profiles are compared with the experimental values. This calculation involves six vibrational modes. The calculated excitation profiles are in excellent agreement, not only with the bandwidth and shape of individual excitation profiles but also with the relative intensities as obtained experimentally. All of the calculated excitation profiles are normalized to the maximum of the ν_1 band. The maxima of all of the calculated excitation profiles are at 28 000 cm^{-1}. The maximum of the absorption band of interest is 28 400 cm^{-1}.

The calculated intensities for all of the observed fundamental, overtone, and combination bands at the excitation wavelength 350.7 nm (ω_l = 28 514 cm^{-1}) are compared to the experimental resonance Raman spectrum in Figure 6. The set of cross sections of excitation profiles for all modes at the laser wavelength 350.7 nm forms the resonance spectrum. The intensities at 350.7-nm excitation in the Raman excitation profiles are represented by vertical broken lines in Figure 5. The Raman intensities for the experimental resonance Raman spectrum are represented by vertical solid lines in Figure 6. The calculated intensities are shown with squares and triangles. The numerical values of the calculated Raman band intensities are compared to the experimental data

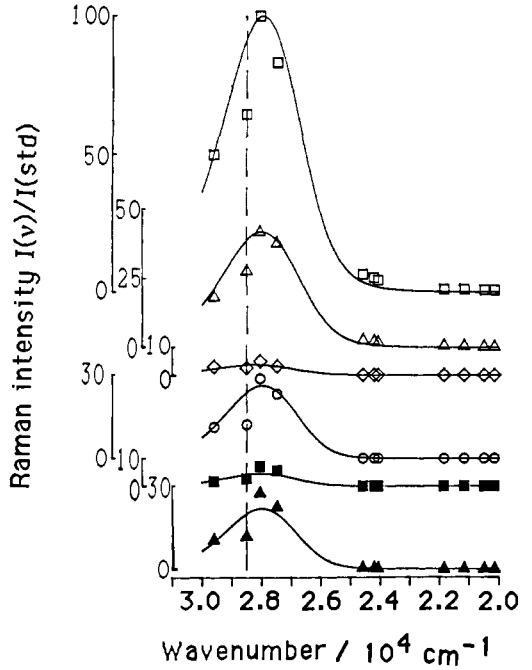

Figure 5. Calculated (—) and experimental resonance Raman excitation profiles of ν_1 (□), ν_2 (△), δ(OCO) (◇), $2\nu_1$ (○), $2\nu_2$ (■), and $\nu_1 + \nu_2$ (▲) for $Rh_2O_2CCH_3(AsPh_3)_2$.

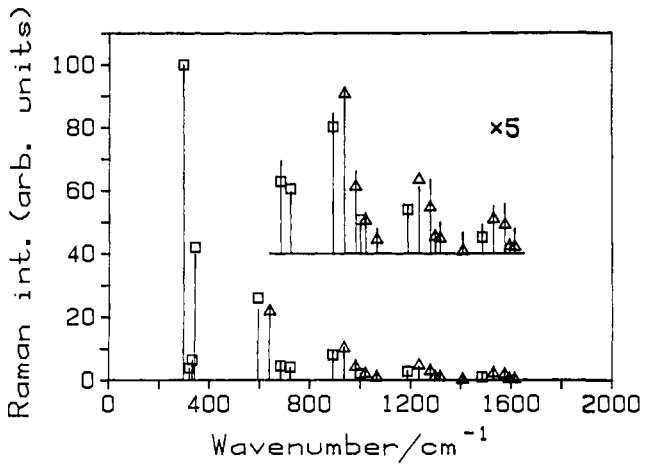

Figure 6. Calculated and experimental resonance Raman spectrum of $Rh_2O_2CCH_3(AsPh_3)_2$ at 350.7-nm excitation: (—) experimental intensities; (□, △), calculated intensities.

in Table III. The calculated Raman intensities are in excellent agreement with those in the experimental spectrum.

The damping factor used in this calculation is 897 cm^{-1}. It is determined by fitting the intensities of the overtone and the combination bands at resonance.

The principal progression-forming mode (ν_1) in the resonance Raman spectrum is almost harmonic up to high quantum number with the anharmonicity constant $x_{11} = -0.16$ cm^{-1}. Other modes show only one or two harmonics. The assumption of an harmonic potential is also reasonable for this molecule.

$Rh_2(O_2CCH_3)_4(SbPh_3)_2$. The best fit excitation profiles of the bands due to the fundamentals ν_1, ν_2, t X-sens, δ(OCO), the overtones $2\nu_1$, $2\nu_2$, and the combinations ν_1 + t X-sens, $\nu_1 + \nu_2$ for $Rh_2(O_2CCH_3)_4(SbPh_3)_2$ are shown in Figure 7. They are calculated by using the parameters in Table I. This calculation involves seven vibrational modes. The calculated excitation profiles for these bands are well matched not only with the bandwidth and shape of each excitation profile but also with the relative intensities determined experimentally. The maxima of the calculated excitation profiles are normalized to the maximum of ν_2, ν(Rh–O), which has the highest intensity. The maxima of the calculated excitation profiles of all modes are at 26 700 cm^{-1}. The maximum of the resonant electronic absorption band is at 27 700 cm^{-1}.

Table III. Calculated and Observed Resonance Raman Intensities for $Rh_2(O_2CCH_3)_4(AsPh_3)_2$

calcd intens[a]	obsd intens	ω_k, cm^{-1}	assignt
100.0	100.0	297	ν_1(Rh–Rh)
3.9	3.9	321	(Rh–O)
6.5	6.5	332	(Rh–O)
42.1	39.7	342	ν_2(Rh–O)
25.9	22.1	593	$2\nu_1$
21.8	23.4	639	$(\nu_1 + \nu_2)$
4.6	5.9	684	$2\nu_2$
4.1	3.9	723	δ(OCO)
8.4	8.9	890	$3\nu_1$
10.1	10.6	935	$(2\nu_1 + \nu_2)$
4.3	5.2	981	$(\nu_1 + 2\nu_2)$
2.2	2.1	1000	p-ring
2.1	2.6	1019	δ(OCO) + ν_1
0.9	1.6	1065	δ(OCO) + ν_2
2.8	2.9	1188	$4\nu_1$
4.7	4.2	1232	$(3\nu_1 + \nu_2)$
2.9	4.7	1276	$(2\nu_1 + 2\nu_2)$
1.1	1.3	1297	p-ring + ν_1
0.9	1.9	1319	δ(OCO) + $2\nu_1$
0.2	1.3	1410	δ(OCO) + $2\nu_2$
1.0	1.8	1481	$5\nu_1$
2.2	3.0	1527	$(4\nu_1 + \nu_2)$
1.8	3.2	1571	$(3\nu_1 + 2\nu_2)$
0.5	0.9	1594	p-ring + $2\nu_1$
0.4	1.6	1615	δ(OCO) + $3\nu_1$

[a] Calculated by using the parameters in Table I.

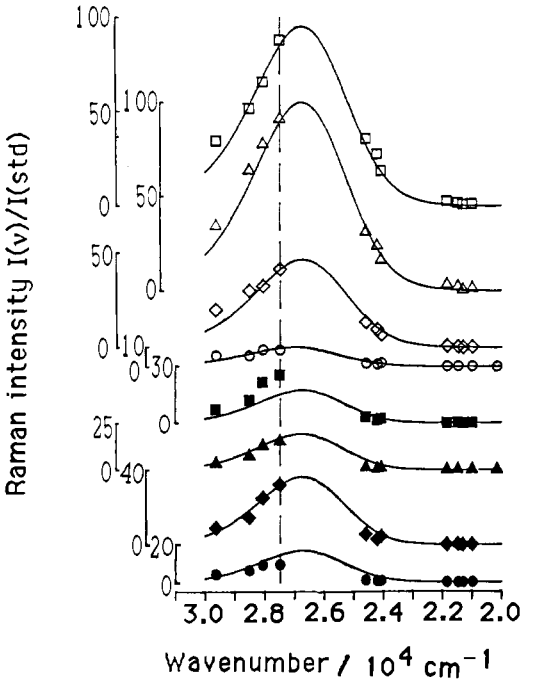

Figure 7. Calculated (—) and experimental resonance Raman excitation profiles of ν_1 (□), ν_2 (△), ν_3 (t X-sens) (◇), δ(OCO) (○), $2\nu_1$ (■), $2\nu_2$ (▲), $\nu_1 + \nu_2$ (♦), $\nu_1 + \nu_3$ (●), for $Rh_2O_2CCH_3(SbPh_3)_2$.

The calculated intensities for all of the observed bands attributable to fundamentals, overtones, and combination tones at the excitation wavelength 363.8 nm (ω_I = 27 488 cm^{-1}) are compared to the experimental resonance Raman data in Figure 8. The set of cross sections of excitation profiles for all modes at the experimental excitation wavelength 363.8 nm forms the resonance Raman spectrum. The intensities at 363.8-nm excitation in the Raman excitation profiles are represented by vertical broken lines in Figure 7. The calculated Raman intensities are represented by squares and triangles in Figure 8. The experimental Raman intensities are represented by vertical solid lines. The numerical

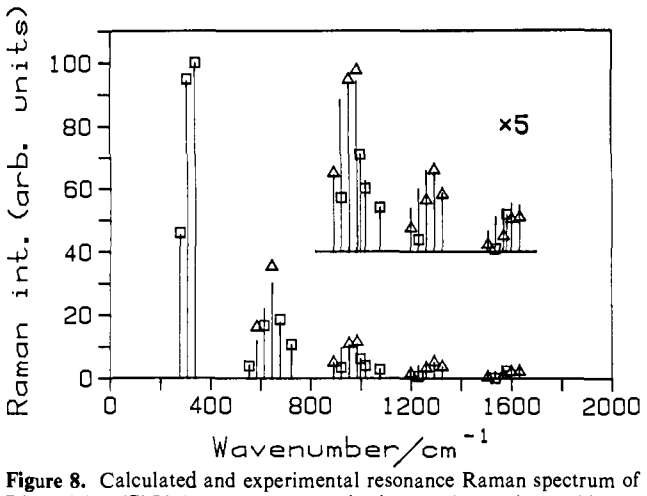

Figure 8. Calculated and experimental resonance Raman spectrum of $Rh_2O_2CCH_3(SbPh_3)_2$ at 363.8-nm excitation: (—) experimental intensities; (□, △) calculated intensities.

Table IV. Calculated and Observed Resonance Raman Intensities for $Rh_2(O_2CCH_3)_4(SbPh_3)_2$

calcd intens[a]	obsd intens	ω_k, cm^{-1}	assignt
45.9	45.3	277	ν_3(t X-sens)
94.8	94.1	307	ν_1(Rh–Rh)
100.0	100.0	339	ν_2(Rh–O)
3.9	4.1	554	$2\nu_3$
16.2	11.8	583	$(\nu_1 + \nu_3)$
16.7	21.9	615	$2\nu_1$
35.3	30.0	645	$(\nu_1 + \nu_2)$
18.6	17.6	678	$2\nu_2$
10.7	10.6	723	δ(OCO)
5.0	4.9	890	$(2\nu_1 + \nu_3)$
3.5	9.6	921	$3\nu_1$
10.9	10.6	952	$(2\nu_1 + \nu_2)$/ν(C–C)
11.5	10.8	983	$(\nu_1 + 2\nu_2)$
6.2	6.2	998	p-ring
4.0	4.5	1016	$3\nu_2$
2.8	2.8	1075	q X-sens
1.5	2.8	1197	$(3\nu_1 + \nu_3)$
0.8	4.0	1228	$4\nu_1$
3.3	5.2	1260	$(3\nu_1 + \nu_2)$
5.2	5.1	1292	$(2\nu_1 + 2\nu_2)$
3.7	3.7	1320	$(\nu_1 + 3\nu_2)$
0.5	1.3	1505	$(4\nu_1 + \nu_3)$
0.2	2.2	1535	$5\nu_1$
1.0	2.7	1566	$(4\nu_1 + \nu_2)$
2.4	2.4	1580	k ν(C–C)
2.1	3.1	1596	$(3\nu_1 + 2\nu_2)$
2.2	2.9	1627	$(2\nu_1 + 3\nu_2)$

[a] Calculated by using the parameters in Table I.

values of calculated Raman band intensities are compared to the experimental data in Table IV. The calculated Raman intensities are in good agreement with those found experimentally. The largest differences between calculated and measured intensities are found for the overtones of ν_1. The difference may be evidence that one of the assumptions made in the calculation is not as valid for this molecule as for the other two molecules studied.

The principal progression-forming mode (ν_1) in the resonance Raman spectrum is harmonic within experimental error with the anharmonicity constant $x_{11} = 0.0$ cm^{-1}. For the stibine complex, ν_2 shows a long overtone progression in the resonance Raman spectrum. This mode is also harmonic, the anharmonicity constant x_{22} being ≤0.1 cm^{-1}. Other modes show only one or two harmonics. Again harmonicity is a reasonable assumption in this calculation.

Quantitative Evaluation of Bond Length and Bond Angle Changes on Excitation. The principal difficulty in attempting to convert from dimensionless displacement units into angstroms lies in knowing what mass to take for the vibrating entities. In the absence of a full force constant analysis for such molecules, it is necessary to fall back on isotopic or pseudoisotopic data for systems $Rh_2(O_2CR)_4(PPh_3)_2$, R = H, CH_3, C_2H_5, or C_3H_7. It is thus important to note that ν_2, ν(Rh–O), for these complexes is very sensitive to the mass of the carboxylate group, falling in the order 402 (H), 338 (CH_3), 332 (CH_3-^{18}O-substituted), 310 (C_2H_5), and 289 (C_3H_7) cm^{-1}. This sensitivity is essentially represented by supposing that each rhodium atom vibrates against half the mass of the carboxylate groups to which it is attached. Thus, if the ν_2 value of 338 cm^{-1} for the case with R = CH_3 is taken as the reference, then the corresponding ν_2 values for the other carboxylate complexes would be 387 (H), 338 (CH_3, reference), 330 (CH_3, ^{18}O-substituted), 304 (C_2H_5), and 278 (C_3H_7) cm^{-1}. It is thus on this basis that the dimensionless coordinates have been converted to angstroms.[21]

Another source of uncertainty in the calculated bond length changes arises from the uncertainties in measuring the peak intensities from the experimental spectrum. A 10% change in bond length causes about a 20% change in the calculated Raman intensities. The reported fits are only obtainable with a much smaller range of values. We conservatively estimate the uncertainty from this cause in the calculated displacement to be ±10%.

In the process of excitation into the lowest allowed electronic transition of $Rh_2(O_2CCH_3)_4L_2$, where L = PPh_3, $AsPh_3$, or $SbPh_3$, the largest bond length changes occur along the Rh–Rh and Rh–O bonds. There are also many coordinates that show small bond length or angle changes upon this excitation, for example, the O–C–O angle bend and those primarily involving phenyl rings.

The Rh–Rh bond length change in $Rh_2(O_2CCH_3)_4L_2$ is 0.047 Å for L = triphenylphosphine, 0.042 Å for L = triphenylarsine, 0.037 Å for L = triphenylstibine. The mass used to convert the dimensionless Δ's into angstrom units for ν(Rh–Rh) is twice of the sum of the masses of rhodium and the axial ligand.[22] The small change in δ(Rh–Rh) of 0.01 Å on going from the PPh_3 to the $SbPh_3$ complex may not be significant since it is not clear the manner in which the effective masses of the vibrating units change with change in the Rh–Rh/Rh–L coupling. However, it should perhaps be noted that the least change on excitation occurs for the $SbPh_3$ complex, for which the Rh–Rh bond is the shortest therefore presumably the strongest.[23,24]

The bond length changes of the Rh–O bonds are more sensitive than those of the Rh–Rh bonds to the axial ligand L. The change in the Rh–O bond length in $Rh_2(O_2CCH_3)_4L_2$ is 0.035 Å for L = triphenylphosphine, 0.041 Å for L = triphenylarsine, and 0.064 Å for L = triphenylstibine. The mass used to convert the dimensionless Δ's into angstrom units for ν(Rh–O) is half of the mass of the acetate group. Because the normal coordinate involves the motion of eight oxygen atoms, the factor $1/(8)^{1/2}$ is multiplied by the value for the normal-coordinate change to calculate the bond length change of an individual Rh–O bond. The Rh–O bond length change in the triphenylstibine complex is quite large compared to that in the triphenylphosphine and triphenylarsine complexes. In fact, in the resonance Raman spectrum of the triphenylstibine complex, the most intense peak is attributed to ν(Rh–O) rather than to ν(Rh–Rh).

The magnitude of the change in the Rh–O bond is surprising on transition to an electronic state which is considered to be σ*(Rh–Rh). However, the metal d_{z^2} orbital, which is the major

(21) The formula to convert the dimensionless displacement Δ into angstroms is

$$\delta = \left(\frac{6.023 \times 10^{23}}{m}\frac{\hbar}{2\pi c\omega}\right)^{1/2} 10^8\Delta$$

where m is the mass involved in the vibration in atomic mass units, ω is the wavenumber of the vibrational mode in reciprocal centimeters, c is the speed of light in centimeters per second, δ is the displacement in angstroms, and Δ is the dimensionless displacement.

(22) If only the masses of the two rhodium atoms are considered, the Rh–Rh bond length change in $Rh_2(O_2CCH_3)_4L_2$ is 0.089 Å for L = triphenylphosphine, 0.085 Å for L = triphenylarsine, and 0.078 Å for L = triphenylstibine.

(23) r(Rh–Rh) is 2.451, 2.427, and 2.421 Å for the complexes $Rh_2(O_2CCH_3)_4L_2$, when L = PPh_3, $AsPh_3$, and $SbPh_3$, respectively.

(24) Clark, R. J. H.; Hempleman, A. J.; Dawes, H. M.; Hursthouse, M. B.; Flint, C. D. *J. Chem. Soc., Dalton Trans.* **1985**, 1775.

component of the Rh–Rh σ interaction, is also σ antibonding with respect to the oxygen atoms. Therefore, the $\sigma \rightarrow \sigma^*$ transition would be expected to change the net Rh–O bond and thus cause the displacement of the Rh–O normal coordinate.

The O–C–O bond angle change in $Rh_2(O_2CCH_3)_4L_2$ is 0.46° for L = triphenylphosphine, 0.92° for L = triphenylarsine, and 1.48° for L = triphenylstibine. To convert the dimensionless Δ's into degrees, only the masses and bond lengths in the O–C–O unit are considered.[25] Because the normal coordinate involves the bending of four O–C–O's, the factor $^1/_2$ is multiplied by the value of normal-coordinate displacement to calculate the individual O–C–O angle change.

There is little or no change of the Rh–Rh–O bond angle based on the Raman intensity. The magnitude of the O–C–O bond angle change is apparently related to the Rh–O bond length change rather than to the Rh–Rh bond length change. If it were related to the Rh–Rh bond length change, the bigger the Rh–Rh bond length change, the greater the O–C–O bond angle change. However, the trend correlates with the Rh–O bond length change. The O–C–O bond angle change has to increase in the order P < As < Sb to accommodate the Rh–O bond length change. These results lead to the conclusion that the position of the carbon atom in the acetate ring is rather fixed in this excitation.

The experimental resonance Raman spectra show no observable intensity for the ν(Rh–L) band where L is P, As, or Sb.[15] One possible interpretation of this result could be the lack of significant displacement along the Rh–L normal coordinate. The time-dependent theory can offer another possibility. The first maximum of the overlap for the fundamental of the low-frequency mode occurs at longer time than that of the high-frequency mode. When the damping factor is high, the magnitude of the overlap of the low-frequency mode suffers more reduction than that of the high-frequency mode. Because ν(Rh–L) is expected to occur at a wavenumber lower than 200 cm^{-1},[15] there can be a significant displacement along the Rh–L coordinate even though no detectable Raman intensity is observed in the experimental spectrum. For example, if the wavenumber of the ν(Rh–Sb) band is 150 cm^{-1} in $Rh_2(O_2CCH_3)_4(SbPh_3)_2$ and the displacement (Δ) of this mode is 0.5, then the resonance Raman intensity at 3638 Å excitation is 0.0049 that of the ν_1 band, which is too small to be detected in the experimental spectrum. The bond length change along the Rh–Sb bond corresponding to $\Delta = 0.5$ is 0.009 Å. (The mass used to convert the dimensionless displacement ($\Delta = 0.5$) into angstroms is the sum of the masses of the Sb atom and three phenyl rings. Because the normal coordinate involves the motion of two $SbPh_3$'s, the factor $1/(2)^{1/2}$ is multiplied by the value of the normal-coordinate displacement to calculate the individual Rh–Sb bond length change.) Therefore, there could be a significant change in Rh–L bond length even though there is no detectable Raman intensity for the ν(Rh–L) band.

The geometric change to the phenyl rings is very small. Therefore, the geometric change to these complexes upon excitation to the resonant state involves almost exclusively the five-membered rings that are formed with the two rhodium atoms and the acetate groups.

The stibine complex undergoes the biggest geometric change upon excitation. This change is shown not only by the Raman intensities but also by the bandwidths of the absorption and the excitation profiles. For the stibine complex, there is a big displacement not only along the Rh–Rh coordinate but also along the Rh–O coordinate upon excitation. Therefore, a long overtone progression of ν_2 is observed. These two coordinates may be coupled to each other in the excited state. This coupling might be the reason why the calculated intensities of the overtone bands arising from ν_1 are in the poorest agreement with those of experiment.

Earlier studies of the depolarization ratio of the ν_1 band of the complexes $Rh_2(O_2CCH_3)_4L_2$, where L = PPh_3, $AsPh_3$, or $SbPh_3$, have shown this to be, in each case, $^1/_3$ at resonance with the lowest allowed electronic transition.[14] This value demonstrates that the transition must be axially polarized[26] and thus $^1A_{2u} \leftarrow {}^1A_{1g}$ in the point group D_{4h}. The most obvious orbital parentage for this transition would be $d_{z^2} \leftarrow d_{z^2}$ (or less probably, $d_{xy} \leftarrow d_{xy}$ or $d_{xz,yz} \leftarrow d_{xz,yz}$), which could account for the long progression in ν_1, ν(Rh–Rh), observed at resonance. However, the significant displacement along ν_2, ν(Rh–O), at resonance suggests that the resonant transition must also have RhO character to it, presumably via π(Rh–O) $\leftarrow d_{xy}$, π(RhO) $\leftarrow d_{xz}$, d_{yz}, and σ(RhO) $\leftarrow d_{z^2}$ parentage.

Summary

The time-dependent theory of resonance Raman spectroscopy has been discussed, and the effects of the most important quantities, the displacement, Δ_k, and the damping factor, Γ, have been described. Both the excitation profiles and the resonance Raman spectra of $Rh_2(O_2CCH_3)_4L_2$ have been accurately calculated. These molecules have significant displacements in the Rh–Rh and Rh–O normal coordinates.

Acknowledgment. This work was made possible by Grant NSF CHE 88-06775 from the National Science Foundation (K.-S.S., J.I.Z.). J.I.Z. also gratefully acknowledges a fellowship from the John Simon Guggenheim Memorial Foundation, which was held in part at University College London.

(25) If the (Rh–O)–C–(O–Rh) unit is considered, the O–C–O angle change in $Rh_2(O_2CCH_3)_4L_2$ is 0.39° for L = triphenylphosphine, 0.78° for L = triphenylarsine, and 1.26° for L = triphenylstibine.

(26) Mortensen, O. S.; Hassing, S. In *Advances in Infrared and Raman Spectroscopy*; Clark, R. J. H., Hester, R. E., Eds.; Heyden: London, 1980; Vol. 6, p 1.